National Aeronautics and Space Administration

Orbital Debris Quarterly News

Volume 26, Issue 3
September 2022

Inside...

On-orbit Fragmentation in July 2
DAS Version 3.2.2 Release 2
HUSIR Radar Measurements of OD Environment: 2021 3
Analysis of ISS-related Returned Surfaces 5
Updates to Thermal Demise Model in ORSAT, Version 7.0 8
New ODPO Logo 10
Conference Report 10
Save the Date for IOC II 11
Space Missions and Satellite Box Score 12

A publication of the NASA Orbital Debris Program Office (ODPO)

International Space Station Maneuvers to Avoid Russian ASAT Fragment

The International Space Station (ISS) conducted a collision avoidance maneuver on 16 June 2022. The avoided object was a large fragment (International Designator 1982-092BYX, Catalog Number 52590) generated from the antisatellite (ASAT) test on Cosmos 1408 by the Russian Federation on 15 November 2021 (ODQN, vol. 26, issue 1, March 2022, pp. 1-5). This ASAT test created more than 1700 fragments large enough to be tracked by the Space Surveillance Network (SSN). Further, it generated significantly more debris too small to be tracked by the SSN but large enough to threaten human spaceflight and robotic missions in low Earth orbit (LEO). Since orbital debris follows a power-law size distribution, mission-ending risk to robotic spacecraft in LEO is driven by millimeter-sized orbital debris. For the ISS, the critical penetration risk for the U.S. modules is dominated by debris approximately 1 cm in size. For the Russian modules, the critical penetration risk is primarily from orbital debris approximately 2 mm in size.

The ISS has experienced many conjunctions with the large, tracked Cosmos 1408 fragments since the ASAT test. This most recent event was the first time the risk of a collision exceeded the requirement for an avoidance maneuver. The ISS has conducted a total of 31 collision avoidance maneuvers since 1999 (see figure). The frequency of the avoidance maneuvers depends on many factors, including solar activity, number of objects crossing the ISS orbit, the tracking capability of the SSN, and others. ♦

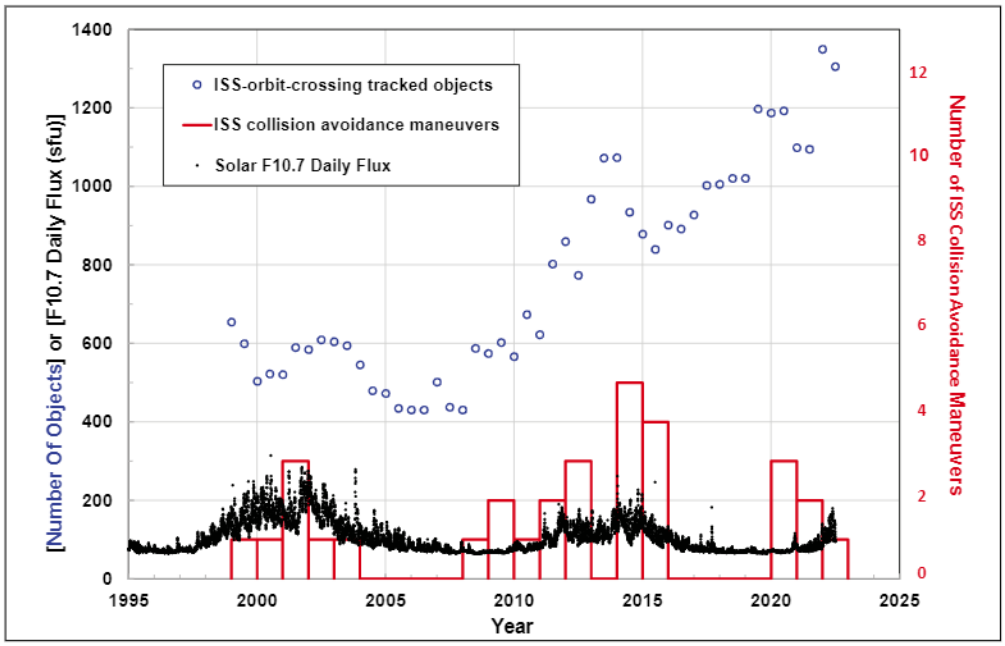

The number of ISS-orbit-crossing objects tracked by the SSN (blue circles), the solar F10.7 daily flux (black dots), and the ISS collision avoidance maneuvers (red histogram) as functions of time.

On-orbit Fragmentation in July

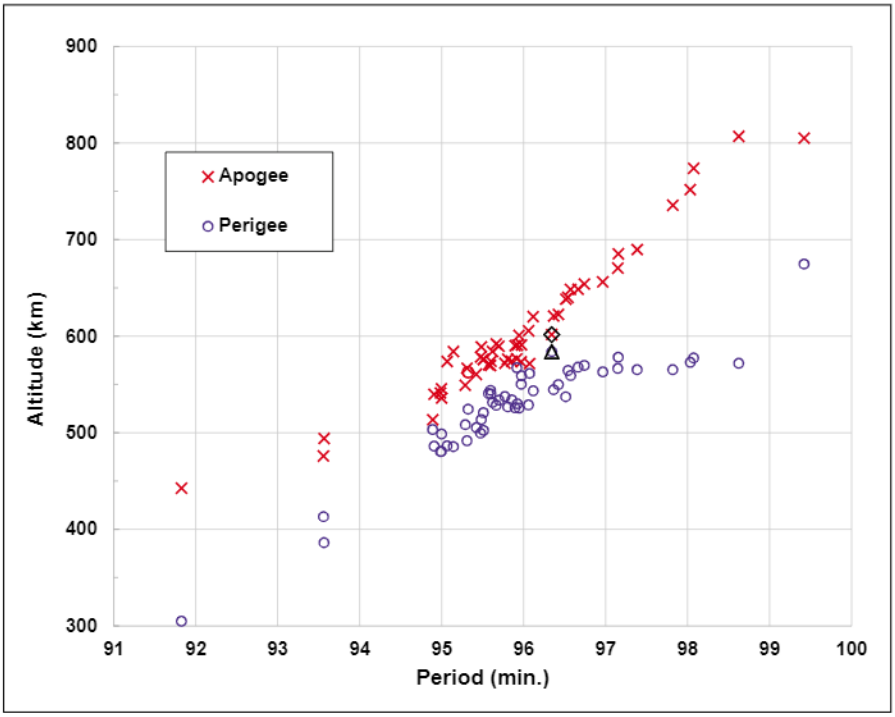

Gabbard diagram of the 2018-084D breakup fragments. Approximate epoch is mid-July 2022. The apogee (black diamond) and perigee (black triangle) altitudes of the parent object, 2018-084D, are also shown.

The 18th Space Defense Squadron (18 SDS) of the U.S. Space Force identified a breakup associated with a mission-related debris (International Designator 2018-084D, Catalog Number 43674) in early July. This mission-related debris was a cylindrical payload fairing cover from a Japanese H-2A upper stage for the deployment of GOSAT-2 and other payloads in October 2018. The breakup occurred at 03:52 ± 0:09 GMT on 03 July 2022. At the time of the breakup, the fairing cover's apogee and perigee altitudes were approximately 615 and 579 km, respectively, with an inclination of 98 degrees. The 18 SDS identified 52 trackable fragments associated with the breakup by late July (see figure). The fairing cover's mass is estimated to be more than 100 kg. It is made of aluminum alloy honeycomb with carbon fiber-reinforced polymer skin. An identical fairing cover from the same GOSAT-2 upper stage also experienced a breakup and generated 74 trackable fragments in July 2020 (ODQN, vol. 24, issue 4, November 2021, pp. 1-2). Since the fairing cover did not appear to contain any energy sources and the 18 SDS' analysis did not show any close conjunctions between 2018-084D and other tracked objects around the time of the breakup, collision with an unknown (small and/or untracked) object is a logical explanation for the breakup. ♦

Debris Assessment Software Version 3.2.2 Release

The NASA Orbital Debris Program Office has released version 3.2.2 of the Debris Assessment Software (DAS), replacing the prior March 2022 release of DAS 3.2.1. This utility provides assessments that can verify compliance of a spacecraft, upper stage, and/or payload with NASA's requirements for limiting debris generation, spacecraft vulnerability, post-mission lifetime, and reentry safety.

This release incorporates updates to the reentry survivability modules and bug fixes for the orbital debris collision and penetration risk assessments.

Successful verification of a design in DAS demonstrates compliance with NASA debris mitigation requirements. Historically, DAS analysis has proven acceptable in meeting compliance requirements of many other agencies in the U.S. and around the world. It does not address the inherent design reliability facets of NASA requirements, but instead addresses all orbital debris requirements that make up the bulk of the requirements in the NASA Technical Standard 8719.14C. To calculate penetration risk from meteoroids, users should consult the NASA Meteoroid Environment Office and Hypervelocity Impact Technology teams for assessments.

For new users, DAS is available for download, by permission only, and requires that an application be completed via the NASA Software Catalog. To begin the process, click on the "Request Software" button in the catalog at https://software.nasa.gov/software/MSC-26690-1.

Users who have already completed the software request process for earlier versions of DAS 3.x do not need to reapply for DAS 3.2.2. Simply go to your existing account on the NASA software portal and download the latest installer. Due to file size limits, the installer is split into several .zip archive files: the main installer and five separate files containing debris environment data. Users must download the main installer, which includes the debris environment for years 2016–2030, and additional environment files required to assess mission years beyond 2030. Approval for DAS is on a per project basis; approval encompasses activities and personnel working within the project scope identified in the application. ♦

SUBSCRIBE to the ODQN or UPDATE YOUR SUBSCRIPTION ADDRESS

To be notified when a new issue of the ODQN is published or to update your email address, subscribe on the NASA Orbital Debris Program Office (ODPO) website at: https://orbitaldebris.jsc.nasa.gov/quarterly-news/

PROJECT REVIEW

HUSIR Radar Measurements of the Orbital Debris Environment: 2021

J. MURRAY and M. MATNEY

The NASA Orbital Debris Program Office (ODPO) uses the Haystack Ultrawideband Satellite Imaging Radar (HUSIR), which is operated by the Massachusetts Institute of Technology's Lincoln Laboratory (MIT/LL), to characterize the distribution of debris in low Earth orbit (LEO). These fragments are smaller than those typically tracked and cataloged by the U.S. Space Command's (USSPACECOM's) Space Surveillance Network (SSN), but they pose a more serious risk to human spaceflight and robotic missions. A summary of these measurements is published annually, with the most recent HUSIR calendar year (CY) 2021 report in review for publication [1]. The data collected is used for the development and validation of debris populations for the ODPO's Orbital Debris Engineering Model (ORDEM). This review article gives an overview of the radar data collected by HUSIR in CY2021, including special observation campaigns targeting debris generated by the Cosmos 1408 anti-satellite (ASAT) test.

For orbital debris radar measurements, HUSIR operates in a beam park mode with the radar pointed at fixed azimuth and elevation angles. Objects are detected as they pass through the radar beam. For orbital debris observations, HUSIR primarily points at 75° elevation due East; a configuration referred to as 75E. The fundamental measurements made by the radar are range, range-rate, and received power from which radar cross section (RCS) can be calculated. Figure 1 shows a plot of the range and range-rate measured for all detections, taken at 75E in CY2021.

Assuming a circular orbit, the inclination of objects traveling through the beam can be estimated from the measured range and range-rate or Doppler velocity. This enables the transformation of the range and range-rate data into orbit altitude and Doppler inclination, as shown in Figure 2. When viewed in this way, several debris families can be identified. The largest is the heavily trafficked sun-synchronous family of orbits clustered about the black dashed curve that represents the sun-synchronous inclinations for circular orbits. Several notable on-orbit fragmentation events are also highlighted by black circles, where the center of each circle denotes the altitude and inclination of the parent body at the time of the event [2]. First seen in HUSIR CY2020 data, a grouping of detections associated with the Starlink constellation at 53°, shown by the black ellipse, is now more pronounced. An additional 925 Starlink satellites were launched into this inclination by SpaceX during CY2021. Also, note that the debris from the Iridium 33 fragmentation has almost completely decayed out of the environment.

The RCS of an object is calculated using the measured power of the reflected signal and the range of the object. Using the NASA Size

continued on page 4

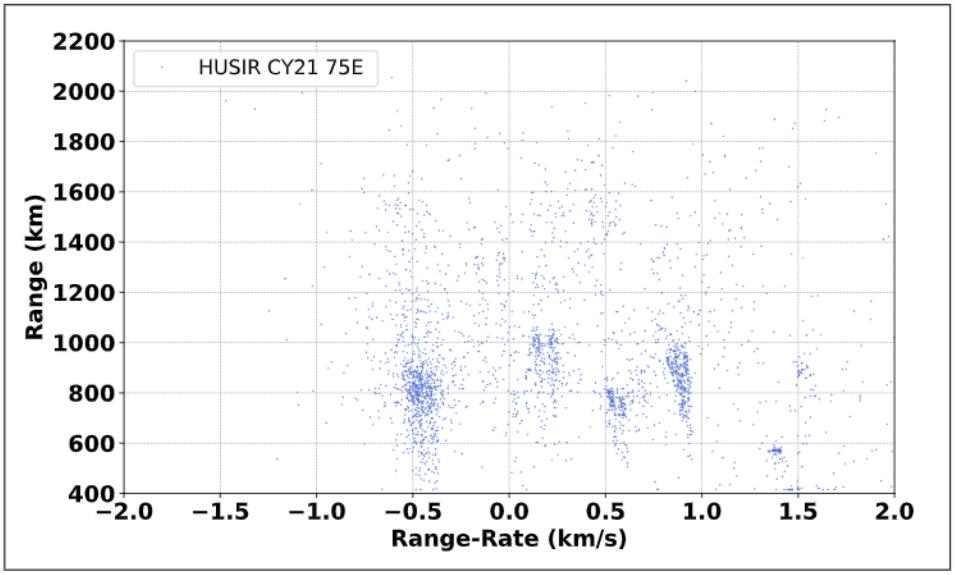

Figure 1. Range versus range-rate observations of resident space objects, as measured by HUSIR in CY2021.

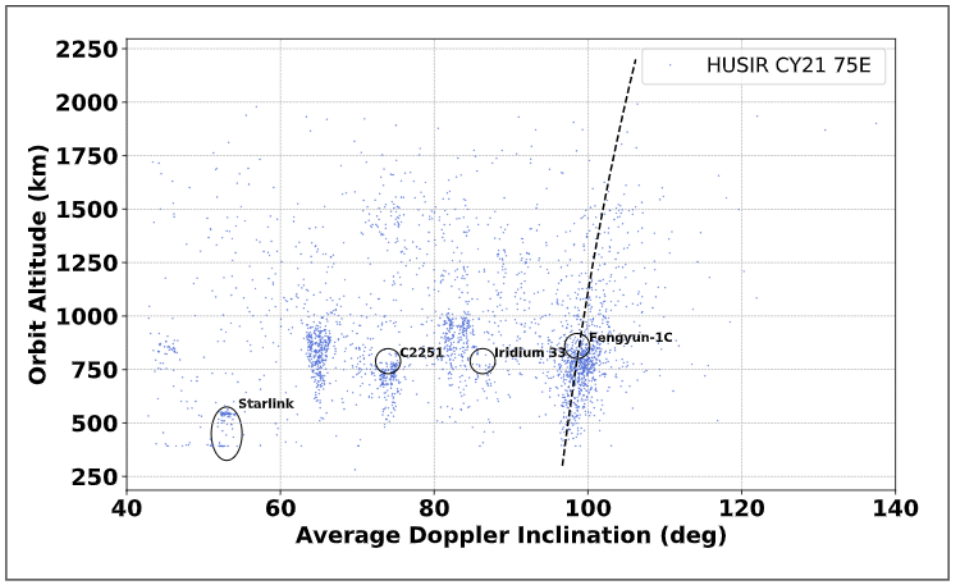

Figure 2. Conversion of HUSIR CY2021 range and range-rate measurements into orbit altitude and Doppler-derived inclination. The sun-synchronous condition, assuming a circular orbit, is shown by the dashed black line.

HUSIR Radar Measurements

continued from page 3

Estimation Model (SEM), the size of a debris object can be estimated from the measured RCS [3]. Figure 3 shows a plot of altitude versus SEM-estimated size for HUSIR detections in CY2021. Also included is a black dashed line depicting the theoretical SEM-size of an object with a single-pulse signal-to-noise ratio (SNR) of 5.65 decibels (dB) as a function of altitude. This curve is calculated using the average sensitivity of HUSIR for CY2021, where 5.65 dB corresponds to the SNR threshold used for detection.

On 15 November 2021, Russia conducted a direct ascent ASAT test that resulted in the breakup of the Cosmos 1408 spacecraft. The outcome of the ASAT test produced over 1700 pieces of large, trackable fragments associated with the catastrophic destruction of Cosmos 1408 (ODQN, vol. 26, issue 1, March 2022, pp. 1-5). To characterize the breakup fragments too small for the SSN to track, the ODPO conducted a measurement campaign over several weeks using both HUSIR and the Goldstone Orbital Debris Radar [4]. It was shown in ODQN, vol. 26, issue 1, March 2022, pp. 1-5 that this data, along with data from other SSN assets, including the Space Fence, closely matches the number of fragments predicted by the NASA Standard Satellite Breakup Model across multiple orders of magnitude in size.

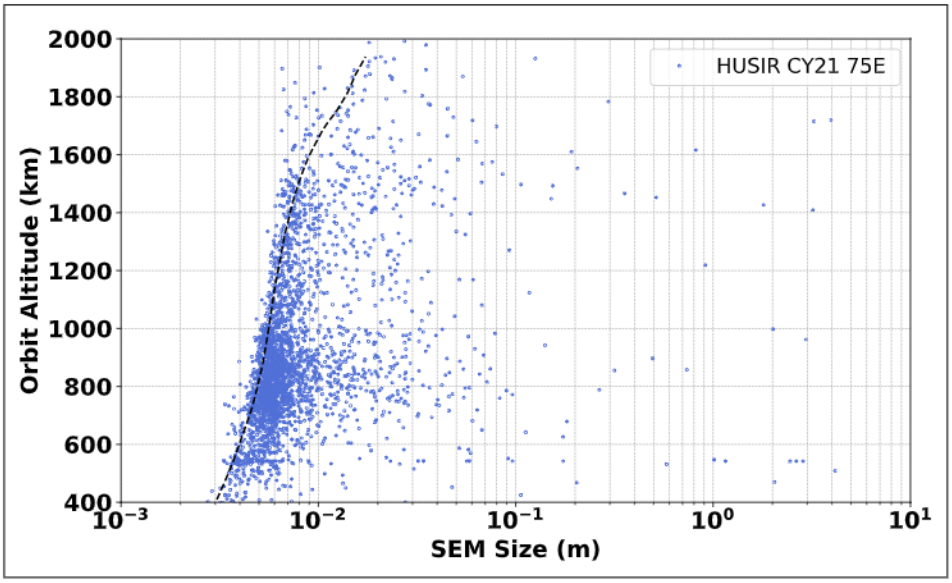

Figure 3. Orbit altitude vs. SEM-size observations of resident space objects, as measured by HUSIR in CY2021. The black dashed line depicts the theoretical SEM-size of an object with a single-pulse SNR of 5.65 dB as a function of altitude.

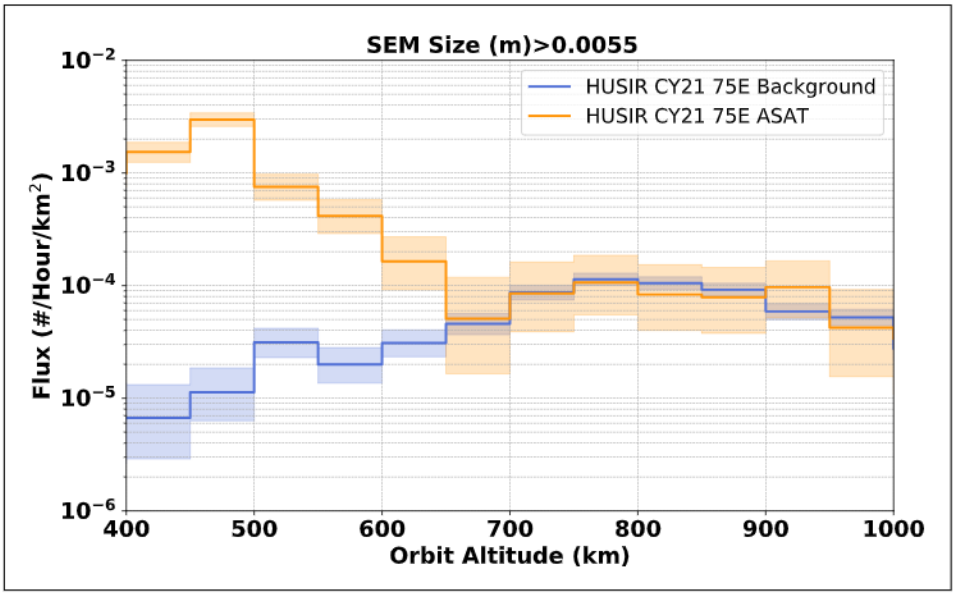

Figure 4. Surface area flux versus altitude of the aggregate HUSIR ASAT observations as compared to the background environment measured in CY21, where flux is limited to objects 5.5 mm and larger. The shaded regions correspond to the 2σ-Poisson confidence intervals. The fluxes presented for the ASAT come from targeted observations. These deliberately enhance the relative contribution from the breakup.

Figure 4 shows the surface area flux versus altitude of the HUSIR ASAT observations compared to contemporaneous background debris environment measurements, where the flux is limited to sizes larger than 5.5 mm. This is the approximate size at which HUSIR measurements are complete at 1000 km altitude and lower. Note that the fluxes presented for the ASAT are derived from targeted observations, which deliberately enhance the relative contribution from the breakup. It does not represent the average flux expected from random observations. The highest flux occurs in the 450 km to 500 km altitude bin, corresponding to the altitude at which the breakup occurred. The flux is elevated above background levels down to the lowest altitude measurable by HUSIR in its standard debris waveform, 400 km, and up to 650 km altitude. Above 650 km, the flux measured in the special data collects was comparable to background levels.

Figure 5 shows the surface area flux versus Doppler inclination of HUSIR ASAT measurements, compared to the background, and limited to altitudes less than 1000 km and sizes larger than 5.5 mm, using 2° wide bins. The flux is elevated above background levels from 74° to 88° inclination, with a peak flux in the 82° to 84° inclination bin, which corresponds to the inclination of the parent body. A more detailed summary and analysis of these measurements can be found in [1, 4].

It is important to note that, although the Cosmos 1408 ASAT occurred in CY2021, its effects are not reflected in the regular CY2021 observation data. Since the event took place late in the CY, 15 November, the debris cloud was still highly localized in time. It did not spread out sufficiently to present itself in statistical sampling data. Additional details are provided in [1]. As the Cosmos 1408 debris cloud spreads, it is expected to become integrated with the background flux in the CY2022 75E dataset.

This article provided a high-level summary of the HUSIR CY2021 radar measurements, with a focus on special observations of the

continued on page 5

HUSIR Radar Measurements

continued from page 4

Cosmos 1408 debris cloud. Continued radar measurements of the orbital debris environment in LEO will continue to characterize small debris fragments of the Cosmos 1408 debris cloud and its evolution over time.

References

1. Murray, J., Matney, M., Kennedy, T. "Haystack Ultra-Wideband Satellite Imaging Radar Measurements of the Orbital Debris Environment: 2021," in review.

2. Anz-Meador, P., *et al*. "History of On Orbit Satellite Fragmentations," 15th Edition, NASA/TM-2018-220037, (2018).

3. Xu, Y.-L. and Stokely, C. "A Statistical Size Estimation Model for Haystack and HAX Radar Detections," 56th International Astronautical Congress, Fukuoka, Japan, (2005).

4. Murray, J., *et al*. "Observations of Small Debris from the Cosmos 1408 Anti-Satellite Test using the HUSIR and Goldstone Radars," 23rd Advanced Maui Optical and Space Surveillance Technologies Conference, Maui, Hawaii, (2022). ♦

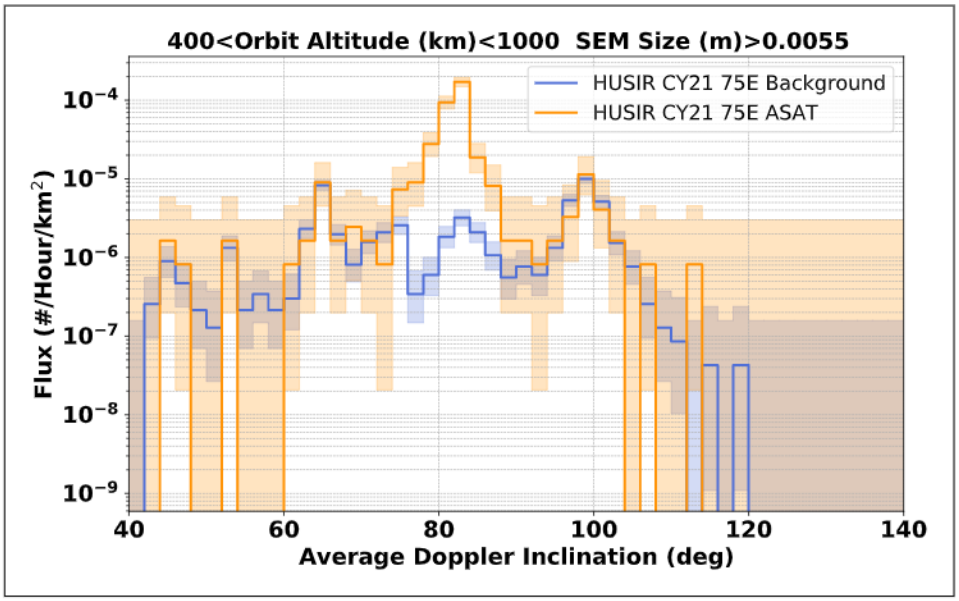

Figure 5. Surface area flux versus Doppler inclination of the aggregate HUSIR ASAT observations as compared to the background environment measured in CY21, where flux is limited to altitudes less than 1000 km and objects 5.5 mm and larger. The shaded regions correspond to the 2σ-Poisson confidence intervals. Note that the fluxes presented for the ASAT are derived from targeted observations, which deliberately enhance the relative contribution from the breakup.

Analysis of ISS-related Returned Surfaces

P. ANZ-MEADOR, M. WARD, J. HYDE, AND E. CHRISTIANSEN

The Orbital Debris Engineering Model (ORDEM) developed by the NASA Orbital Debris Program Office (ODPO) is a data-driven model – extensive radar, optical, laboratory, and *in situ* measurement data sets have been used to build the model since its earliest versions. A salient aspect of professional software development is the verification and validation (V&V) process. Verification answers the question "Is the model built correctly?" while validation addresses the question "Did we build the correct model?" Less extensive, reserved, or independent data sets serve the validation requirement. For example, samples from the Hubble Space Telescope (HST) provided validation data sets for the development of ORDEM 3.1 (ODQN, vol. 24, issue 2, April 2020, pp. 2-4) and of ORDEM 3.2, the current release version. Unfortunately, due to the dynamic nature of the orbital debris environment, data can grow stale relatively quickly and new sources are required to both build and validate ORDEM development.

In addition to the HST's relatively higher-altitude data sets, *in situ* data collected at and near the International Space Station (ISS) supplies both build data (Space Shuttle Orbiter Vehicle impact data) and validation data. This project review updates a prior characterization (ODQN, vol. 20, issue 3, July 2016, pp. 4-6; and ODQN, vol. 22, issue 1, February 2018, pp. 4-5) of ISS soft goods, the Pressurized Mating Adapter 2 (PMA-2) blanket and examines a recent limited-scope feasibility study conducted on the Space Exploration Technologies Corp. (SpaceX) Dragon capsule's Thermal Protection System (TPS) material.

The PMA-2 blanket was exposed to the space environment between 09 July 2013 and 25 February 2015. See Figure 1 for an on-orbit photograph of a PMA blanket. The approximately 3.7 m²-area blanket is composed of a betacloth outer layer and multiple ballistic fabric inner layers. Figure 2 depicts a penetration feature identified in the woven

continued on page 6

Figure 1. The ISS Node 3 axial port's PMA-3 cover. The PMA-2 cover, on the Harmony module's PMA, is otherwise identical, though no on-orbit imagery appears to exist. Credit: NASA photo #iss035e037061

Returned Surfaces

continued from page 5

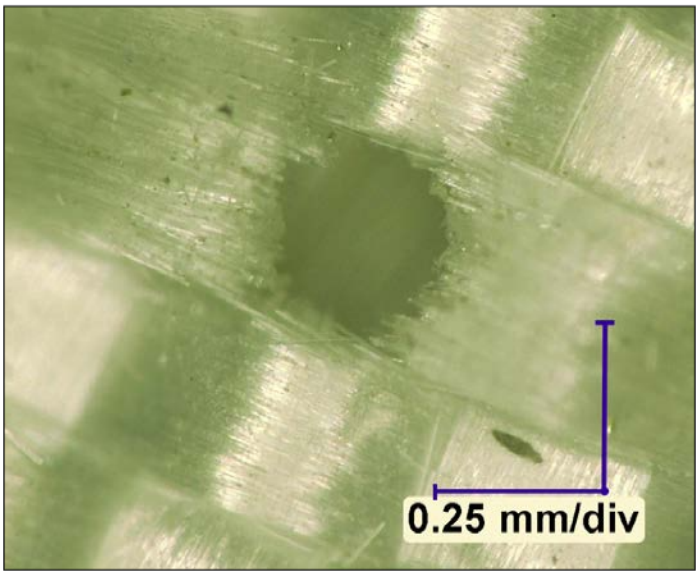

Figure 2. Microphotograph of a PMA-2 blanket penetration.

Figure 3. The SpaceX Dragon capsule flown on the Commercial Resupply Mission 17 (CRS-17). The conical capsule's lateral surface is SPAM TPS material. Credit: NASA photo #iss059e043284

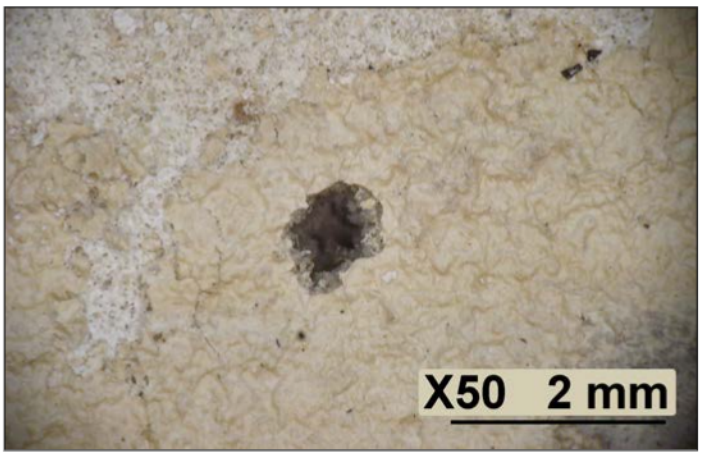

Figure 4. CRS-17 SpaceX Dragon capsule MMOD damage on and into SPAM TPS.

beta cloth blanket; in this analysis, a penetration refers to the severing of a complete thread bundle, and smaller features, while likely present, remain to be examined.

The SpaceX Cargo Dragon capsule regularly visited the ISS from 2012 through 2020 and potentially provides a timely and well-characterized source of data for modeling purposes. The capsule's lateral surfaces use SpaceX Proprietary Ablative Material (SPAM) TPS material for thermal management during all mission phases (Figure 3) and is regularly surveyed for micrometeoroid and orbital debris (MMOD) damage post-flight (Figure 4) by members of NASA's Hypervelocity Impact Technology (HVIT) group. SPAM is a syntactic foam TPS material.

A fundamental requirement for any analysis of *in situ* materials is the high-probability identification of residues found in the impact feature as either MM or OD (or unknown) so as to segregate these populations for statistical assessment purposes. Scanning Electron Microscope (SEM)/Energy Dispersive X-Ray (EDX) analysis of impact features can resolve the question by finding residue constituent elements and, based on analyst experience, identifying the materials as high-likelihood MM, OD, or unknown.

HVIT personnel extracted PMA-2 blanket material samples by stamping them out of the blanket using a circular punch. SpaceX personnel supplied SPAM core samples to HVIT for analysis, and these supply the samples examined in this work. In the case of PMA-2 sampling, the samples chosen comprise an ensemble of damage features approximately 0.5 mm in size and larger; the three largest SPAM damage features were similarly chosen for the feasibility study reported here.

Table 1 describes and characterizes SEM/EDX analysis outcomes. Of the 11 samples investigated, 2 were determined to be MM and the remainder were identified to have constituents that were associated with OD. In the table, "SS" connotes stainless steel. All outcomes are considered high density constituents in the ODPO mass density classification scheme.

Table 1. PMA-2 Blanket Sampling Analysis

PMA-2 sample number	Largest Damage dimension (mm)	Result (MM, OD, or Unknown)	Constituents
1	0.62	OD	SS, ZnS, Ti
2	1.19	OD	SS, NiO
4	0.60	OD	Zn, Fe
7	0.55	OD	Ti and Fe, Ti and S, Ba and S
8	0.60	OD	Fe, Cr, Mn, SS, Fe & Ni
10	0.93	OD	SS, Fe
12	0.73	MM	Ca, Mg, Fe, S, O
13	0.75	MM	Fe, Ni, S
23	0.61	OD	Fe, Cu, Ti
24	0.37	OD	SS, TiO, FeO
25	0.58	OD	Ti, Fe+Cu, Mo, Co, Fe, Cr, Ni

continued on page 7

Returned Surfaces

continued from page 6

Table 2. SpaceX SPAM TPS Sampling Analysis

CRS Mission ID	Sample Number	Largest Damage dimension (mm)	RESULT (MM, OD, or Unknown)	Constituents
CRS-13	211	4.79	OD	Fe, Cr, Ni (or SS), Ba, Calcite
CRS-15	226	4.15	MM	S, Fe, Ni
CRS-18	273	3.635	OD	Pt, Pt & Fe, Cu & Zn, Zr and Ca

Table 2 similarly describes SEM/EDX outcomes for the three SPAM samples. Again, all sample outcomes fall into ODPO's high density category.

A second fundamental requirement for analysis of *in situ* materials is a means of correlating damage feature size and the size of the MMOD particle that created it; this is calculated using damage equations derived with ground-based hypervelocity impact testing and hydrocode simulations, which have historically given a basis of estimate for impactor size. In both the case of the PMA-2 betacloth and the SPAM materials, a simple linear relationship between particle and impact feature size is indicated and used here.

Figure 5 presents a size distribution for all samples examined in this work, with sample number called out explicitly, and including one sigma sampling uncertainties. The two ensembles are remarkably consistent given sampling and interpretation uncertainties.

The combined number-size distribution data, as presented in Figure 5, will be separated by impactor type (MM or OD). The computations used to calculate OD flux use detailed exposure and pointing information that is available for these surfaces to provide a validation data set for ORDEM development.

The SPAM samples were evaluated under a limited feasibility study to determine if the cored impactor samples would serve as good candidates for timely *in situ* measurements of the orbital debris environment. Study outcomes show that impactor residues are present within impact features in observable quantities and can be characterized as either MM or OD using standard SEM/EDX techniques. A simple damage equation yields results consistent, at the number-size distribution level, with the PMA-2 outcomes.

The PMA-2 outcomes are noteworthy from several perspectives. Prior to the analysis, the expectation was that the number of MM and OD would be statistically equal at ISS altitudes for the size range of impacts analyzed here (ODQN, vol. 22, issue 1, February 2018, Fig. 7, p. 5). However, nine OD to two MM outcomes may indicate a sampling bias. This is further suggested by the relative preponderance of high density (> 6 g/cm^3) constituents versus medium (2-6 g/cm^3) and low (< 2 g/cm^3) mass density constituents. This may indicate a betacloth-related sampling bias, a hypothesis currently being explored. Additionally, noted in this review is the paucity of titanium (Ti) alloys in aerospace applications, the most prevalent being alloyed with aluminum or vanadium, neither of which were explicitly identified here. This may suggest that Ti represents a paint pigment particle rather than a bulk debris object in the usual sense.

The research presented in this article exemplifies the continued collaboration between NASA's ODPO, HVIT, and Astromaterials Research Offices to assess returned surfaces that support ORDEM development. ♦

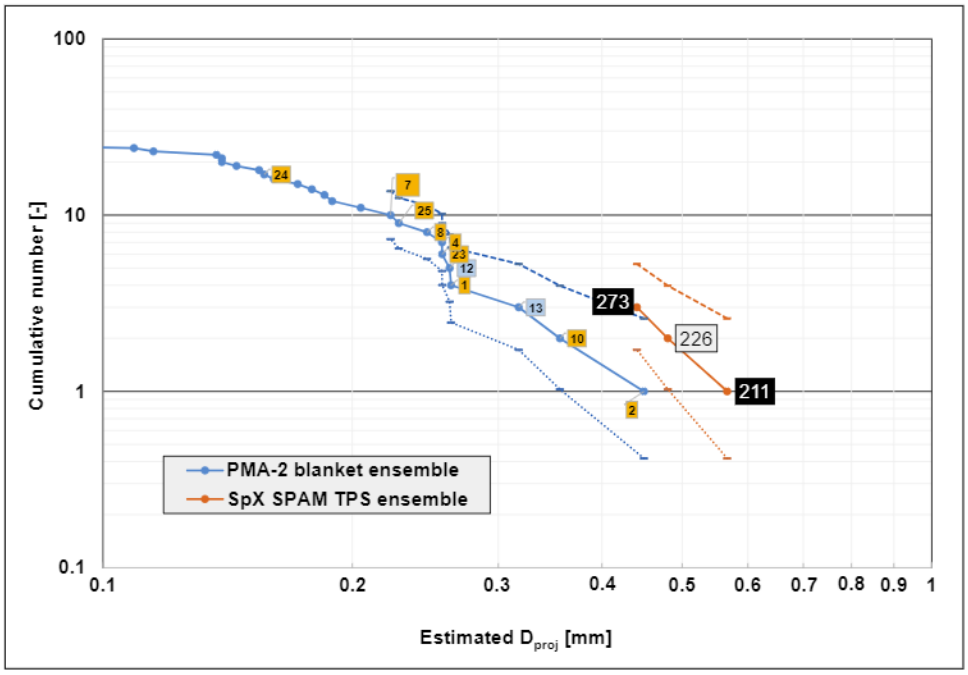

Figure 5. Cumulative number as a function of estimated projectile diameter, D_{proj}. PMA-2 orange/yellow flags indicate OD assessments with sample number while light blue flags denote MM. SPAM black flags show OD assessment while the sole MM assessment, sample 226, is represented by a gray flag. One sigma Poisson sampling uncertainties are indicated by dashed and dotted lines for both ensembles.

The NASA Orbital Debris Photo Gallery has high resolution, computer-generated images of objects in Earth orbit that are currently being tracked. Photos and graphics may be freely downloaded from the NASA Orbital Debris Program Office webpages, unless they include a third-party credit line. In these cases, permission must be granted by the copyright owner. The Photo Gallery link is: https://orbitaldebris.jsc.nasa.gov/photo-gallery/.

Updates to Thermal Demise Model in Object Reentry Survival Analysis Tool, Version 7.0

B. GREENE, C. OSTROM, AND J. MARICHALAR

As an increasing number of spacecraft and launch vehicle upper stages opt for fiber-reinforced polymer (FRP) components over more traditional aluminum or steel, it is critical to understand the reentry demise process of these modern materials to continue accurately predicting the human casualty risk from uncontrolled space structure reentry. Earlier studies by the NASA Orbital Debris Program Office (ODPO), discussed in ODQN, vol. 23, no. 3, August 2019, pp. 3-5 and in [1], and another study [2] have shown that many FRP materials tend to pyrolyze into a sturdy matrix of fibers and charred resin that resists shredding by aerodynamic forces and can even act as a thermal shield for components embedded inside. This behavior is not captured using the thermal demise models included in the most recent operational version of the Object Reentry Survival Analysis Tool (ORSAT), 6.2.1.

Figure 1. Image of carbon fiber-reinforced polymer sample coupon under test at the University of Texas Inductively Coupled Plasma (ICP) Torch Facility. Courtesy of Colin Yee, graduate student on the UT project, reproduced with permission.

The ODPO performed Phase II of its FRP reentry demise testing in August 2019 (ODQN, vol. 23, no. 2, April 2020, pp. 5-6) and used this data to develop a new thermal demise model for ORSAT 7.0 that includes charring of the resin matrix in FRPs. Figure 1 shows a photograph of the laboratory setup in operation. This model is based on a model for fire damage to carbon fiber-reinforced polymer (CFRP) [3]. The results of a test implementation of the model were presented by the ODPO [4].

The ODPO is currently finalizing ORSAT 7.0, which includes a fully functional version of the new thermal demise and pyrolysis models. The full ORSAT 7.0 release with associated documentation is expected in Fiscal Year 2023. In addition to more accurately modeling FRP demise, these models have many other benefits including simplicity, improved numerical stability, extensibility to new object shapes, and the ability to accurately model proprietary resin mixtures and fiber weave combinations using easily obtainable thermogravimetric analysis (TGA) data.

The new thermal demise model in ORSAT 7.0 is a complete re-architecture of earlier versions. ORSAT 6.2.1 and its predecessors used a 1-D conduction model with shape-dependent conductor coefficients, which required a separate partial differential equation integrator to be written for each type of shape primitive supported by ORSAT. In ORSAT 7.0, this model is replaced with a forward-time/center-space numerical integration scheme for the full variable-property, variable-cross-section, 1-D thermal diffusion equation implemented on a non-uniform mesh. In addition, it allows new shape primitives to be defined by specifying a new equation for the 1-D mesh cell volume and cross-section. Due to these enhancements and improved numerical stability, the pre-release build of ORSAT 7.0 appears to run slower than the current version. The goal for ORSAT 7.0 is to ensure proper demisabilty factors for RFPs and new shape primitives. Computational improvements will be investigated in future releases.

Modeling the pyrolysis of FRP resin is done using a temperature-varying density. The model [4] calculates the density as a function of peak temperature using a lookup table or Arrhenius relation derived from TGA data. Since running a TGA analysis is rapid and inexpensive, it can be used to characterize any proprietary resin/fiber/weave combination a spacecraft or rocket manufacturer may use.

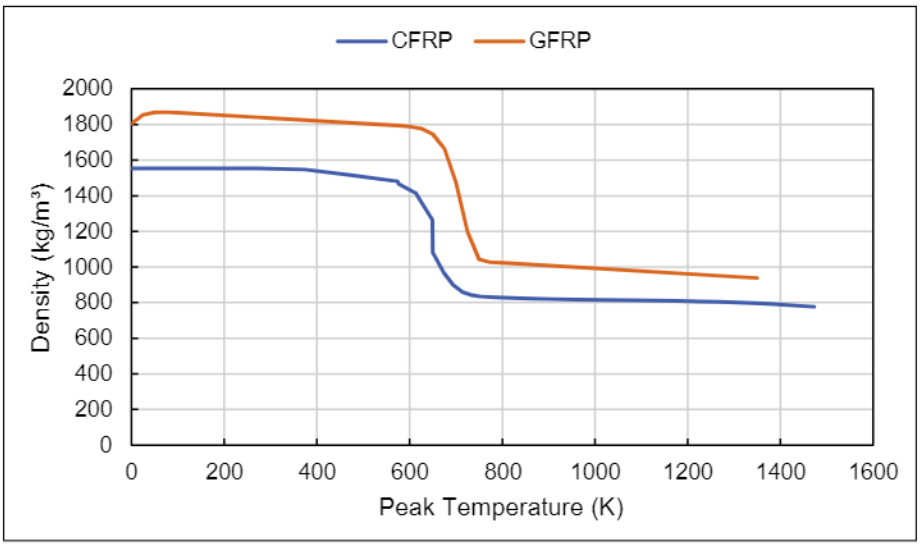

Figure 2. Modeled density of the CFRP and GFRP material as a function of peak temperature.

For general analysis of charring CFRP and glass fiber-reinforced polymers (GFRPs), ORSAT 7.0 includes two new built-in material models: a carbon fiber-reinforced epoxy matrix and a G10/FR4 glass fiber-reinforced polyester matrix. Both new models include pyrolysis of the polymer matrix and melting/sublimation of the fiber material. The material density for both models as a function of peak temperature, derived from thermogravimetric analysis performed for the ODPO by the thermal design branch at the

continued on page 9

Updates to ORSAT v7

continued from page 8

NASA Johnson Space Center, is shown in Figure 2.

The specific heat and thermal conductivity for CFRP were derived from measurements presented by [5], which was the best reference for these values in a woven laminate CFRP found in the literature. Little research could be found regarding high-temperature behavior of GFRP. Based on comparing the room-temperature values for various types of GFRP from reference [6] with those for CFRP from reference [5], it is assumed the thermal conductivity for GFRP is half that of the CFRP model.

To validate these models, a sample coupon of each material was modeled in ORSAT 7.0 and subjected to a cold wall heat flux of 21 W/cm². The coupon was modeled as 80 mm long, 25 mm wide, and 10 mm thick with a flow velocity of 7516 m/s at an altitude of 95 km. The modeled temperatures and char depth were compared to several tests performed during the ODPO's Phase II FRP demisability study [4]. Figure 3 shows a comparison of the char depth for CFRP modeled in ORSAT to that seen in an off-the-shelf CFRP coupon under similar thermal conditions. Figure 4 shows the same comparison for GFRP.

In Figure 3, the modeled char depth closely matches the char depth measured in the Phase II test coupon after a short ramp-up period of 7 seconds. Most likely, this difference in the first few seconds is due to the surface texture of the sample coupon, which is not modeled in ORSAT. The char depth of the GFRP model and sample coupon, on the other hand, match closely for the first 10 to 15 seconds, but then the model begins to overpredict the char depth by about 20%. Presumably, this is because ORSAT also predicted a much more rapid surface recession due to melting and spallation of the glass fibers than was seen in the Phase II test. The flow velocity in the University of Texas Inductively Coupled Plasma (ICP) Torch Facility is not high enough to cause significant spallation of the molten glass, so melted layers of glass can act as an insulator against the plasma, slowing the observed rate of char progression.

These results show that the new thermal demise and charring model in ORSAT 7.0 matches test data obtained by the ODPO in earlier test campaigns. Further validation of the new ORSAT 7.0 models is currently in work. These new models will improve the accuracy of thermal demise predictions for FRP material fragments on modern spacecraft.

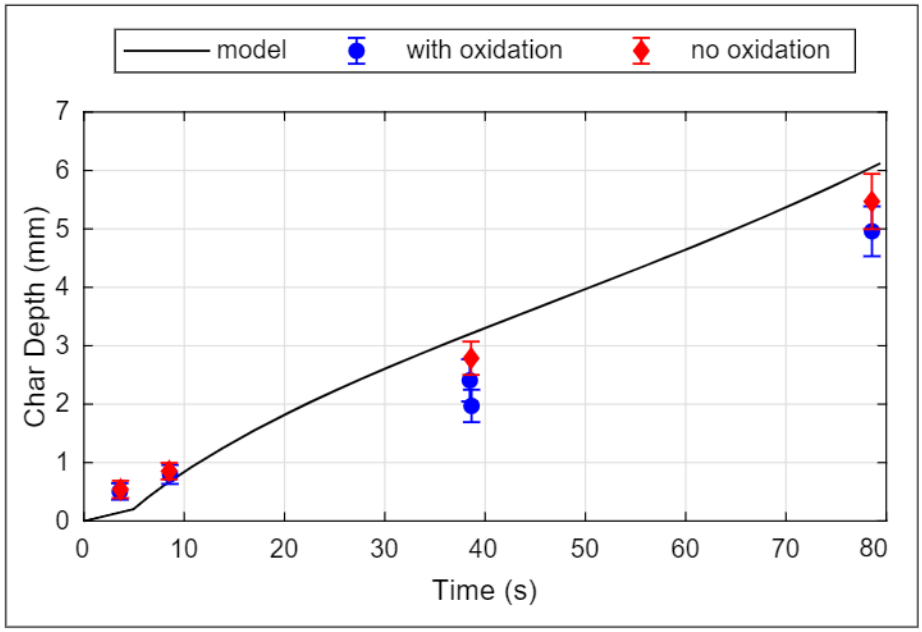

Figure 3. Comparison of modeled char depth over time for CFRP as modeled in ORSAT 7.0 and a sample coupon of the same material and shape exposed to a 20W/cm² plasma flow.

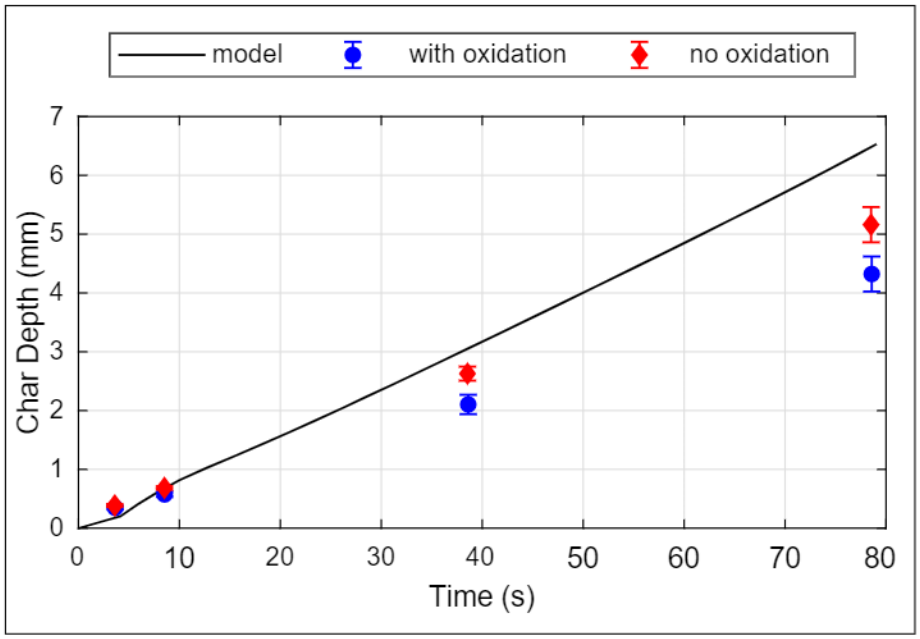

Figure 4. Comparison of modeled char depth over time for GFRP as modeled in ORSAT 7.0 and a sample coupon of the same material and shape exposed to a 20W/cm² plasma flow.

References

1. Greene, B. and Sanchez, C. "Demisability of GFRP and CFRP Components of Reentering Orbital Debris: Phase I Test Results," in 10th International Association for the Advancement of Space Safety Conference, El Segundo, CA, May 15-17, 2019.

2. Lips, T., *et al.*, "About the Demisability of Propellant Tanks During Atmospheric Re-Entry from LEO," in 8th International Association for the Advancement of Space Safety Conference, Melbourne, FL, 2016.

3. Di Modica, P., "Modelling Fire Behaviour of Composite Materials," School of Mechanical and Systems Engineering, Newcastle University, 2016.

continued on page 10

Updates to ORSAT v7

continued from page 9

4. Greene, B. and Ostrom, C. "Pyrolysis Rate and Yield Strength Reduction in Carbon Fiber and Glass Fiber Composites Under Reentry Heating Conditions," in 8th European Conference on Space Debris, Darmstadt, Germany, 2021.

5. Tranchard, P., *et al.*, "Modelling Behaviour of a Carbon Epoxy Composite Exposed to Fire: Part I - Characterisation of Thermophysical Properties," Materials, vol. 10, no. 4, pp. 494-513, 2017.

6. Spurgeon, W. "Thermal Conductivities of Some Polymers and Composites," US Army Research Laboratory, Aberdeen Proving Ground, MD, 2018.

7. Greene, B. and Sanchez, C. "Demisability of GFRP and CFRP Components of Reentering Orbital Debris: Phase I Test Results," in 10th International Association for the Advancement of Space Safety Conference, El Segundo, CA, 2019. ♦

New ODPO Logo

The NASA Orbital Debris Program Office (ODPO) is a Delegated Program in the NASA Headquarters' Office of Safety and Mission Assurance (OSMA). ODPO has updated its logo for identification at international conferences, for print media, and for public outreach. In this redesigned logo, emphasis is placed on ODPO's three primary roles: measurements, modeling, and mitigation.

ODPO collects a wide variety of measurements to statistically assess the dynamic orbital debris environment, including optical, radar, *in situ*, and laboratory measurements. The measurement data collected provides the basis for ODPO's environmental models and tools.

ODPO develops, maintains, and upgrades orbital debris models to describe and characterize the current and future debris environment. These models are used to assess risk to operational spacecraft and upper stages; to study the evolution of the debris environment; and to investigate how the future debris environment will change under various mitigation and remediation practices. ODPO-developed tools are also used to compute object reentry survivability and predict risk to people on the ground.

ODPO leads the development of national and international orbital debris mitigation standards and best practices to preserve the near-Earth space environment for the long-tern sustainability of outer space activities. ODPO developed the first set of NASA orbital debris mitigation requirements in 1995 and supports OSMA to evaluate Orbital Debris Assessment Reports and End of Mission Plans to ensure NASA mission compliance with the requirements.

The new logo highlights the importance ODPO assigns to controlling the growth of the orbital debris population. In the center, representative debris in low Earth orbit (LEO) surrounds our planet. This illustrates the high concentration of debris populations in LEO. The dots, exaggerated in size, represent spacecraft (active and retired), spent upper stages, and other debris large enough to be tracked and cataloged, although there are many more debris objects too small to track that still pose a threat to operational spacecraft.

We introduce our new logo as a digital ambassador representing ODPO and the orbital debris policies that ODPO supports. ♦

CONFERENCE REPORT

Meteoroids 2022 Conference, 13-17 June 2022 (Virtual)

Meteoroids 2022 was the 11th international conference in a triennial series of meetings on meteoroids, their origins, and their associated phenomena. This year, the meeting was hosted by the Universities Space Research Association, the Lunar Planetary Institute, and NASA's Meteoroid Environment Office. Meteoroid impacts pose a risk to spacecraft and upper stages analogous to that of orbital debris. In addition to scientific knowledge, meteoroid studies provide important data used for spacecraft safety and mission assurance.

The virtual 2022 meeting featured live invited talks for each session; pre-recorded versions of submitted talks, with a small time slot for questions and answers; and online poster sessions. The pre-recorded talks let attendees view the presentations at their leisure before or after the session. In all, more than 140 participants from 27 countries were able to hear and to discuss the results that the researchers presented in more than 125 different talks and posters.

A survey of the session titles highlights the diversity of the topics covered:

- Meteoroid sources
- Composition and physical properties
- Dust particles and clouds in the solar system and beyond

continued on page 11

Meteoroids 2022

continued from page 10

- *In-situ* experiments and spacecraft anomalies
- Dynamical evolution
- Meteor shower dynamics and the 2021 Arids
- Human-generated debris
- Meteor physics and chemistry
- Meteor spectra, luminous efficiency, and meteorite analysis
- Meteorite recoveries
- Influx of interplanetary and interstellar material

Because the meteor community is quite small, yet globally distributed, a career fair was organized to introduce researchers to employment and post-doctoral opportunities in meteors and related fields. Details about this conference can be found at: https://www.hou.usra.edu/meetings/meteoroids2022/contacts/. The next Meteoroids conference is planned for Perth, Australia, in 2025. ♦

UPCOMING MEETINGS

Save the Date for IOC II

Purpose and Scope

The goal of the 2nd International Orbital Debris Conference (IOC) is to promote orbital debris research activities in the United States and to foster collaborations with the international community. The 4-day conference will cover all aspects of meteoroid and orbital debris research, mission support, and other related activities.

Topics

- Measurements: radar, optical, *in situ*, laboratory, *etc.*
- Modeling: engineering, long-term environment, near-term risk assessments, reentry, *etc.*
- Operations and mission support: hypervelocity impact and protection, satellite anomalies, conjunction assessments, *etc.*
- Environment management: mitigation, remediation, space traffic coordination, policy, *etc.* ♦

SATELLITE BOX SCORE

(as of 4 August 2022, cataloged by the U.S. SPACE SURVEILLANCE NETWORK)

Country/ Organization	Spacecraft*	Spent Rocket Bodies & Other Cataloged Debris	Total
CHINA	556	3814	4370
CIS	1557	6416	7973
ESA	96	59	155
FRANCE	82	517	599
INDIA	107	112	219
JAPAN	205	121	326
UK	479	1	480
USA	5011	5219	10230
OTHER	1108	96	1204
TOTAL	9201	16355	25556

* *active and defunct*

Visit the NASA
Orbital Debris Program Office Website
www.orbitaldebris.jsc.nasa.gov

Technical Editor
Heather Cowardin, Ph.D.

Managing Editor
Debi Shoots

Correspondence can be sent to:
Robert Margetta
robert.j.margetta@nasa.gov
or to:
Nilufar Ramji
nilufar.ramji@nasa.gov

National Aeronautics and Space Administration
Lyndon B. Johnson Space Center
2101 NASA Parkway
Houston, TX 77058

www.nasa.gov
https://orbitaldebris.jsc.nasa.gov/

INTERNATIONAL SPACE MISSIONS

01 April 2022 – 30 June 2022

Intl.* Designator	Spacecraft	Country/ Organization	Perigee Alt. (KM)	Apogee Alt. (KM)	Incli. (DEG)	Addnl. SC	Earth Orbital R/B	Other Cat. Debris
1998-067	ISS dispensed debris	Various	411	417	51.6	0	0	2
2022-033A	OMNI-L1	US	623	641	97.9	37	0	0
2022-034B	GLOBAL-18	US	427	435	53.0	0	2	1
2022-034C	GLOBAL-20	US	426	436	53.0			
2022-035A	GAOFEN 3 03	PRC	750	752	98.4	0	1	0
2022-036A	COSMOS 2554	CIS	901	910	67.2	0	1	0
2022-037A	AXIOM-1	US	225	402	51.6	0	0	1
2022-038A	CHINASAT 6D	PRC	35778	35795	0.0	0	1	0
2022-039A	DAQI 1	PRC	700	701	98.1	0	1	0
2022-040A	USA 327	US	1013	1209	63.5	0	0	0
2022-041A	STARLINK-3810	US	538	541	53.2	52	0	4
2022-042A	DRAGON FREEDOM	US	413	420	51.6	0	0	0
2022-043A	SUPERVIEW NEO-1 01	PRC	486	501	97.5	0	1	6
2022-043C	SUPERVIEW NEO-1 02	PRC	481	506	97.5			
2022-044A	COSMOS 2555	CIS	117	135	96.4	0	0	0
2022-045A	STARLINK-3889	US	539	541	53.2	52	0	4
2022-046A	JILIN-01 GAOFEN 4A	PRC	527	545	97.5	4	1	0
2022-047A	SPACEBEE-143	US	518	530	97.5	25	1	0
2022-048A	JILIN-01 KUANFU 01C	PRC	529	545	97.7	7	0	0
2022-049A	STARLINK-3870	US	538	541	53.2	52	0	4
2022-050A	TIANZHOU 4	PRC	379	388	41.5	0	1	2
2022-051A	STARLINK-3951	US	538	542	53.2	52	0	4
2022-052A	STARLINK-4019	US	539	541	53.2	52	0	4
2022-053A	STARLINK-4004	US	539	541	53.2	52	0	4
2022-054A	COSMOS 2556	CIS	503	514	97.7	0	1	0
2022-055A	CST 100 STARLINER 2	US	414	422	51.6	0	0	0
2022-056A	OBJECT A	PRC	866	898	86.0	0	1	0
2022-056B	OBJECT B	PRC	988	1057	86.0			
2022-056C	OBJECT C	PRC	870	895	86.0			
2022-057A	LEMUR 2 TENNYSONLILY	US	522	536	97.5	45	0	0
2022-058A	OBJECT A	PRC	600	617	50.0	8	1	0
2022-059A	PROGRESS MS-20	CIS	413	420	51.6	0	1	0
2022-060A	SZ-14	PRC	379	388	41.5	0	1	4
2022-061A	NILESAT 301	EGYP	35777	35796	0.0	0	1	0
2022-062A	STARLINK-4091	US	458	460	53.2	52	0	4
2022-063A	SRH3	GER	745	747	98.4	0	0	0
2022-064A	GLOBALSTAR FM15	US	1111	1126	52.0	3	0	1
2022-064B	USA 328	US	NO INITIAL ELEMENTS					
2022-065A	PVSAT	SKOR	694	709	98.0	6	1	0
2022-066A	TIANXING-1	PRC	280	298	96.8	0	1	0
2022-067A	CMS-02	IND	35754	35819	0.0	0	1	1
2022-067B	MEASAT 3D	MALA	35787	35788	0.0			
2022-068A	YAOGAN-35 D	PRC	492	502	35.0	0	1	1
2022-068B	YAOGAN-35 E	PRC	489	504	35.0			
2022-068C	YAOGAN-35 F	PRC	490	504	35.0			
2022-069A	GAOFEN 12 (03)	PRC	627	630	98.0	0	1	0
2022-015D	NACHOS-1	US	394	403	51.6	0	0	0
2022-070A	CAPSTONE	US	EN ROUTE TO MOON			0	1	0
2022-070C	LUNAR PHOTON	US	HIGH EARTH ORBIT					
2022-071A	SES-22	SES	35777	35796	0.0	0	1	0
2022-072A	DS-EO	SING	564	572	10.0	0		
2022-072B	OBJECT B	TBD	561	571	10.0			
2022-072C	NEUSAR	SING	560	573	10.0			
2022-072D	OBJECT D	TBD	528	561	10.0			
2022-072E	OBJECT E	TBD	531	582	10.0			

* *Intl. = International; SC = Spacecraft; Alt. = Altitude; Incli. = Inclination; Addnl. = Additional; R/B = Rocket Bodies; Cat. = Cataloged*
Notes: 1. Orbital elements are as of data cut-off date 30 June. 2. Additional spacecraft on a single launch may have different orbital elements. 3. Additional uncatalogued objects may be associated with a single launch.